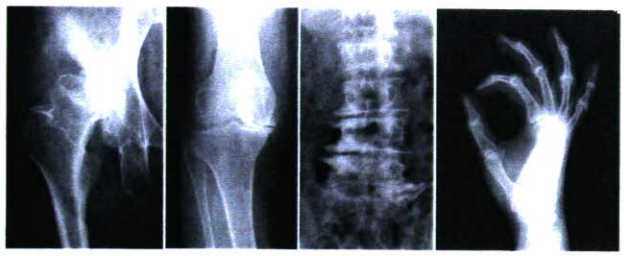

Fig. 1. Radiographs of osteoarthritis (OA) in hip, knee, lumbar spine, and hand. Cartilage degradation shown as joint space narrowing and osteophyte formation at the edge of the joints are two major disorders of OA.

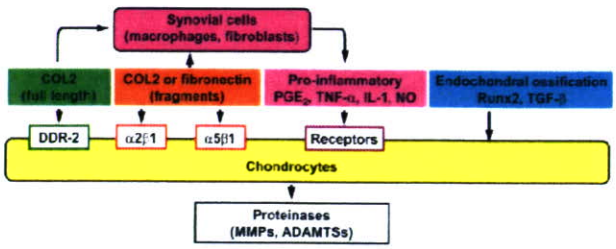

Fig. 2. Upstream signals of the induction of proteinases in chondrocytes. Matrix proteins, pro-inflammatory factors, and endochondral ossification signals are principal pathways.

plateau (Glasson et al., 2007, *ibid*). We have developed the medial model by resection of the medial meniscus and medial colateral ligament (Kamekura et al., 2005). In addition, there is a traditional anterior cruciate ligament transection (ACLT) model that has also been used in larger animals (Clements et al., 2003).

Proteinases for OA induction

Normal joint cartilage is constituted of a framework of type II collagen (COL2), in which proteoglycans connected to hyaluronic acid waves smoothly. Because proteoglycans contain a large quantity of water, they provides elasticity and lubricity to the joint surface. However, in the OA cartilage, most of the proteoglycans are cut, fragmented, and floating in the synovial fluid. Due to the loss of the shock-absorber, the mechanical stress is loaded directly onto COL2, which is also cut and degraded. It has been shown that the initiation of OA occurs with the appearance of proteinases such as matrix metalloproteinases (MMPs) and aggrecanases that sever the core proteins of proteoglycans at their specific cleavage sites (Little et al., 2007). Actually, the importance of a proteinase, ADAMTS5, also called aggrecanase-2, was proved by back-to-back publications in 2005 (Glasson et al., 2005; Stanton et al., 2005), creating a DMM model in knockout mice which showed resistance to cartilage degradation under the OA induction. However, the clinical trials of the proteinase inhibitors for the OA treatment have not been successful due to side effects like musculoskeletal pain, tendinitis, and so on (Burrage et al., 2007; Nagase et al., 2006). Hence, researchers are now turning their attention to the signals inducing the proteinases in chondrocytes; Figure 2 summarizes the upstream signals that may cause this induction. Olsen's group and others have shown that matrix protein, especially undegraded COL2, may initiate it through a receptor tyrosine kinase discoidin domain receptor 2 (DDR-2) (Li et al., 2007; Xu et al., 2005; 2007). This causes the degradation of matrix proteins, and the product fragments of COL2 or fibronection then induce proteinases through respective integrins $\alpha 2\beta 1$ and $\alpha 5\beta 1$ (Li et al., 2007).

Pro-inflammatory factors and OA

Besides these matrix proteins, pro-inflammatry factors like prostaglandins (PGs), tumor necrosis factor-α (TNF-α), interleukin-1 (IL-1), IL-6, and nitric oxides are reported to induce proteinases through their respective receptors (Vincenti et al., 2002). These pro-inflammatory factors are also reported to be produced by synovial cells under the stimulation of the undegraded or fragmented matrix proteins (Li et al., 2007). However, it is suspected that these cytokines play significant roles in the OA development. Our previous report showed that levels of TNF-α, IL-1, IL-6 as well as fibroblast growth factor-2 in the synovial fluid from knee joints of OA patients were much lower than those of rheumatoid arthritis patients (Manabe et al., 1999). Furthermore, a previous report using a mouse ACLT model showed that mice lacking IL-1, IL-1-converting enzyme, stromelysin 1 or inducible nitric oxide synthase unexpectedly exhibited an acceleration of cartilage degradation, implying that these pro-inflammatory factors do not stimulate, but rather inhibit such degradation (Clements et al., 2003).

PGE_2, a representative pro-inflammatory factor, is produced more abundantly in the OA cartilage than in normal cartilage (Jacques et al., 1999), and microsomal PGE synthase-1 (mPGES-1) is a terminal enzyme for the PGE_2 production in chondrocytes of OA patients (Kojima et al., 2004). Although we created the medial OA model in the PGES-1 knockout mice, the cartilage degradation and osteophyte formation were comparable to the wil-type littemates (Yamakawa et al., 2008) (Fig. 3). We therefore believe that inflammation may be associated with the OA process as a consequence, but might not have a central role in the cause of OA initiation or progression.

Chondrocyte hypertrophy and OA

Our examination of the time course of histology of the

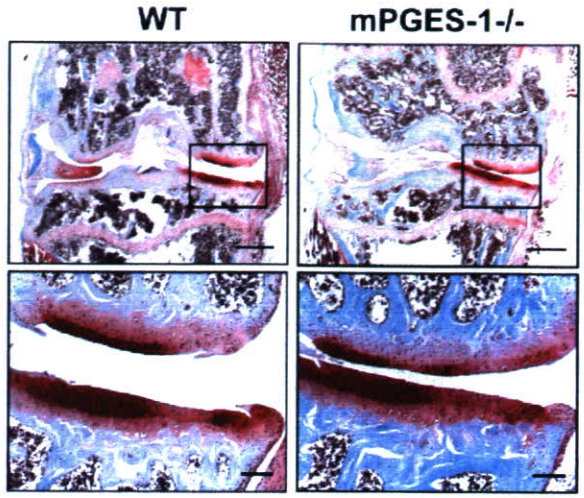

Fig. 3. Cartilage degradation in the medial portion of tibial cartilage during the OA development in the mouse medial model (Safranin O staining). Eight-week-old male WT and mPGES–/– mice underwent medial collateral ligament transaction and medial meniscus resection in the right knee joint. The inset boxes indicate the regions of the lower panels. Bars, 500 μm (upper) & 50 μm (lower).

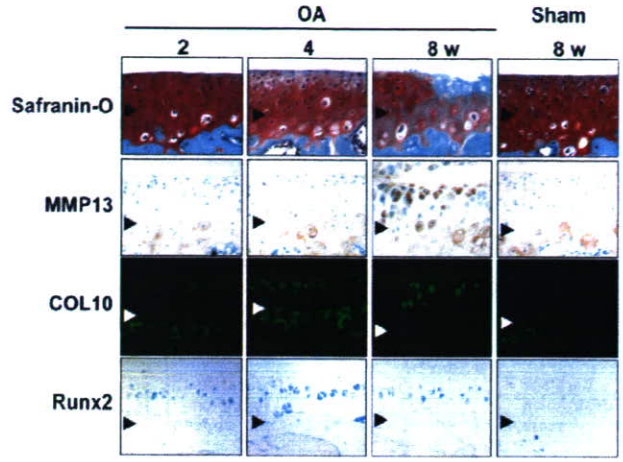

Fig. 4. Time course of expressions of MMP-13, COL10, and Runx2 in the medial tibial cartilage of OA-induced and sham-operated knee joints in the mouse medial model. Localization of MMP-13 and COL10 was detected by immunohistochemistry, and Runx2 localization was detected by X-gal staining of heterozygous Runx2 deficient mice with LacZ knock-in at the site of Runx2 deletion (Runx2+/lacz). Arrowheads indicate the level of tidemark.

mouse joint cartilage using the medial OA model revealed that type X collagen (COL10) and MMP-13 were significantly induced during OA progression (Fig. 4) (Kamekura et al., 2005; 2006). COL10 expression, a specific marker of hypertrophic chondrocytes, appeared in the superficial and middle zones above the tidemark at 4 weeks, consistent with previous studies (Boos et al., 1999; von der Mark et al., 1992). MMP-13 expression appeared in the hypertrophic chondrocytes above the tidemark at 8 weeks. These findings suggest that articular chondrocytes undergo hypertrophic differentiation in response to joint instability, and the hypertrophic chondrocytes express MMP-13 that may degrade the cartilage matrix.

Since a transcriptional activator Runx2 has been known to induce both chondrocyte hypertrophy and MMP-13 expression (Jimenez et al., 1999; Takeda et al., 2001; Ueta et al., 2001), we then examined the involvement of Runx2 during OA development (Kamekura et al., 2006). Runx2 expression was induced above the tidemark in the cartilage as early as 2 weeks, enhanced at 4 weeks, and decreased thereafter by the OA induction, which was not observed in the sham-operated cartilage (Fig. 4). For the functional analyses of Runx2, we used heterozygous Runx2-knockout mice (Runx2+/–), since homozygous Runx2-knockout (Runx2–/–) mice died just after birth. The Runx2+/– mice showed normal skeletal development and articular cartilage under physiological conditions. Both COL10 and MMP-13 expressions were decreased by the Runx2 insufficiency (data not shown), indicating that chondrocyte hypertrophy and MMP-13 induction during OA progression is at least partly mediated by Runx2. When the OA progression was compared between WT and Runx2+/– joints, the cartilage degradation in Runx2+/– was much milder than that of the WT cartilage at 8 weeks and thereafter (Fig. 5A). The Runx2+/– joint also showed decreased osteophyte formation (Fig. 5B). These findings demonstrate that Runx2 contributes to cartilage degradation and the subsequent osteophyte formation under joint instability.

Our differential display analysis identified a novel molecule that was up-regulated by a high phosphate diet in association with calcification of auricular cartilage in mice, and we called it carminerin (Koshizuka et al., 2003; Okawa et al., 1998). The knockout (carminerin –/–) mice did not show skeletal abnormality under physiological conditions. When we created the ACLT OA model, the joint destruction normally occurred; however, osteophyte formation seemed to be decreased by the knockout, indicating that carminerin is not essential for cartilage degradation but plays a role in osteophyte formation (Fig. 6) (Yamada et al., 2006).

Chondrocyte apoptosis and OA

In addition to hypertrophic differentiation of chondrocytes, chondrocyte apoptosis is known to be involved in OA development (Kühn et al., 2004). Intraarticular injection of a pan-caspase inhibitor has been reported to suppress cartilage degradation under OA induction in a rabbit

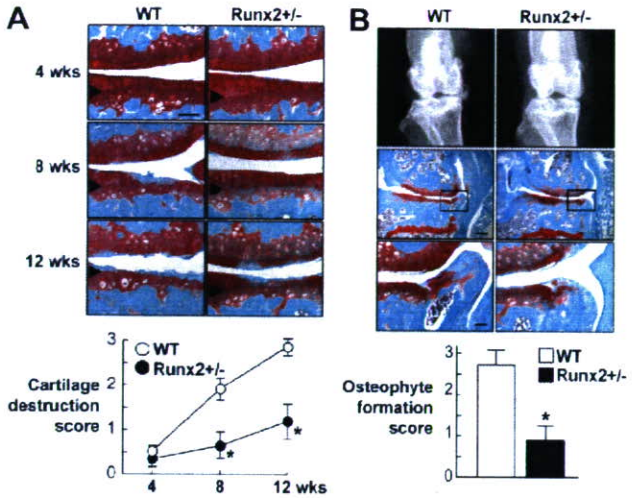

Fig. 5. A. Safranin-O staining and the cartilage degradation score of the medial tibial cartilage of Runx2–/– and wild-type (WT) littermates. Arrowheads indicate the level of tidemark. **B.** Anteroposterior X-ray features, Safranin-O staining, and the osteophyte formation score 12 weeks after surgery. Means (symbols or bars) ± SEM (error bars). * $P < 0.01$ vs. WT.

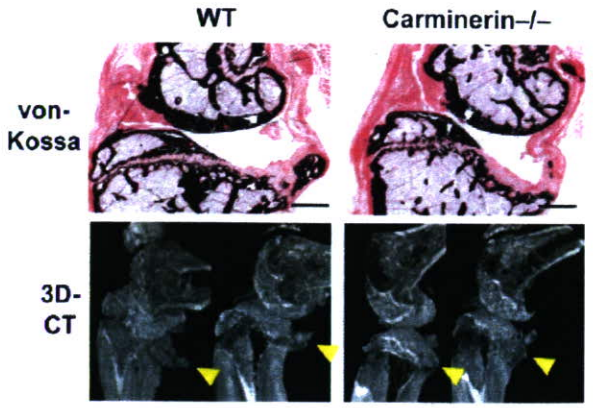

Fig. 6. von Kossa staining and three-dimensional computed tomography (3D-CT) of knee joints of carminerin–/– and wild-type (WT) littermates in the ACLT model. OA was induced at the posterior tibias of the knee joint of 8-week-old mice and examined 10 weeks after surgery.

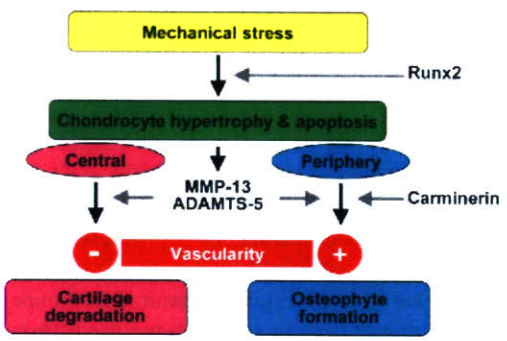

Fig. 7. Molecular background of OA progression under mechanical stress by mouse genetics approaches.

ACLT model (D'Lima et al., 2006). When we created the OA medial model in the hetero knockout mice of osteoprotegerin that is well known as a decoy receptor of RANKL for osteoclastic bone resorption, joint destruction was enhanced as compared to the wild-type littermates (Shimizu et al., 2007). On the contrary, an intraarticular injection of recombinant osteoprotegerin suppressed joint destruction with a decrease of apoptotic chondrocytes. Since tumor necrosis factor-related apoptosis-inducing ligand (TRAIL), a ligand of osteoprotegerin, induces chondrocyte apoptosis (Lee et al., 2004; Pettersen et al., 2002), osteoprotegerin might inhibit the apoptosis induced by TRAIL. These *in vivo* findings clearly demonstrate that not only chondrocyte hypertrophy, but also chondrocyte apoptosis, both of which are signals of endochondral ossification, play some roles in cartilage degradation during OA development under mechanical stress.

Conclusion

Figure 7 summarizes our hypothessis of the molecular background of OA progression under mechanical stress in joints. As the mechanism involved in this stress causing protease production, in addition to matrix proteins and pro-inflammatory signals, we hereby propose the importance of chondrocyte hypertrophy and apoptosis, which are signals for endochondral ossification. The proteinases produced by hypertrophic chondrocytes cause cartilage degradation at the center of the joint and osteophyte formation at the periphery. The difference of the two sites may depend on the vascularity. At the periphery, vascularity is accessible from synovium or tendon, which causes endochondroal ossification to occur and make osteophytes, just like at the growth plate. Carminerin may play a role in the chondrocyte calcification at this stage. However, in the center, the vascularity is not accessible from the edge, so that it ends up with cartilage degradation without being replaced by bone.

The ultimate aim of our study is to identify the molecular targets for clinical treatment of OA. Although we primarily used mouse genetics approaches, we have attempted to confirm the reproducibility of the mouse findings in humans as well through human gene polymorphism or clinical biochemical studies. Among the molecules introduced in this review, there are some whose suppression ameliorated skeletal disorders under pathological conditons but did not affect physiological conditions, indicating that the treatment targeting these molecules may lead to an ideal treatment without side effects on physiological functions. In fact, clinical trials based on the present findings are currently being practically planned.

References

Bluteau, G., Gouttenoire, J., Conrozier, T., Mathieu, P., Vignon, E., Richard, M., Herbage, D., and Mallein-Gerin, F. (2002). Differential gene expression analysis in a rabbit model of osteoarthritis induced by anterior cruciate ligament (ACL) section. Biorheology *39*, 247–258.

Boos, N., Nerlich, A.G., Wiest, I., von der Mark, K., Ganz, R., and Aebi, M. (1999). Immunohistochemical analysis of type-X-collagen expression in osteoarthritis of the hip joint. J. Orthop. Res. *17*, 495–502.

Burrage, P.S. and Brinckerhoff, C.E. (2007). Molecular targets in osteoarthritis: metalloproteinases and their inhibitors. Curr. Drug Targets *8*, 293–303.

Clements, K.M., Price, J.S., Chambers, M.G., Visco, D.M., Poole, A.R., and Mason, R.M. (2003). Gene deletion of either in-terleukin-1beta, interleukin-1beta-converting enzyme, inducible nitric oxide synthase, or stromelysin 1 accelerates the development of knee osteoarthritis in mice after surgical transection of the medial collateral ligament and partial medial meniscectomy. Arthritis Rheum. *48*, 3452–3463.

D'Lima, D., Hermida, J., Hashimoto, S., Colwell, C., and Lotz, M. (2006). Caspase inhibitors reduce severity of cartilage lesions in experimental osteoarthritis. Arthritis Rheum. *54*, 1814–1821.

Glasson, S.S., Askew, R., Sheppard, B., Carito, B., Blanchet, T., Ma, H.L., Flannery, C.R., Peluso, D., Kanki, K., Yang, Z., et al. (2005). Deletion of active ADAMTS5 prevents cartilage degradation in a murine model of osteoarthritis. Nature *434*, 644–648.

Glasson, S.S., Blanchet, T.J., and Morris, E.A. (2007). The surgical destabilization of the medial meniscus (DMM) model of osteoarthritis in the 129/SvEv mouse. Osteoarthritis Cartilage *15*, 1061–1069.

Glasson, S.S. (2007). *In vivo* osteoarthritis target validation utilizing genetically-modified mice. Curr. Drug Targets *8*, 367–376.

Hayami, T., Pickarski, M., Wesolowski, G.A., McLane, J., Bone, A., Destefano, J., Rodan, G.A., and Duong, le T. (2004). The role of subchondral bone remodeling in osteoarthritis, reduction of cartilage degeneration and prevention of osteophyte formation by alendronate in the rat anterior cruciate ligament transection model. Arthritis Rheum. *50*, 1193–1206.

Jacques, C., Sautet, A., Moldovan, M., Thomas, B., Humbert, L., and Berenbaum, F. (1999). Cyclooxygenase activity in chondrocytes from osteoarthritic and healthy cartilage. Rev. Rhum. Engl. Ed. *66*, 701–704.

Jimenez, M.J., Balbin, M., Lopez, J.M., Alvarez, J., Komori, T., and Lopez-Otin, C. (1999). Collagenase 3 is a target of Cbfa1, a transcription factor of the runt gene family involved in bone formation. Mol. Cell. Biol. *19*, 4431–4442.

Kamekura, S., Hoshi, K., Shimoaka, T., Chung, U., Chikuda, H., Yamada, T., Uchida, M., Ogata, N., Seichi, A., Nakamura, K., et al. (2005). Osteoarthritis development in novel experimental mouse models induced by knee joint instability. Osteoarthritis Cartilage *13*, 632–641.

Kamekura, S., Kawasaki, Y., Hoshi, K., Shimoaka, T., Chikuda, H., Maruyama, Z., Komori, T., Sato, S., Takeda, S., Karsenty, G., et al. (2006). Runx2 contributes to pathogenesis of osteoarthritis in mice after induction of knee joint instability. Arthritis Rheum. *54*, 2462–2470.

Kojima, F., Naraba, H., Miyamoto, S., Beppu, M., Aoki, H., and Kawai, S. (2004). Membrane-associated prostaglandin E synthase-1 is upregulated by proinflammatory cytokines in chondrocytes from patients with osteoarthritis. Arthritis Res. Ther. *6*, R355–365.

Koshizuka, Y., Yamada, T., Hoshi, K., Ogasawara, T., Chung, U., Kawano, H., Nakamura, Y., Nakamura, K., Ikegawa, S., and Kawaguchi, H. (2003). Cystatin 10, a novel chondrocyte-specific protein, may promote the last steps of the chondrocyte differentiation pathway. J. Biol. Chem. *278*, 48259–48266.

Kühn, K., D'Lima, D.D., Hashimoto, S., and Lotz, M. (2004). Cell death in cartilage. Osteoarthritis Cartilage *12*, 1–16.

Le Graverand, M.P., Eggerer, J., Vignon, E., Otterness, I.G., Barclay, L., and Hart, D.A. (2002). Assessment of specific mRNA levels in cartilage regions in a lapine model of osteoarthritis. J. Orthop. Res. *20*, 535–544.

Lee, S.W., Lee, H.J., Chung, W.T., Choi, S.M., Rhyu, S.H., Kim, D.K., Kim, K.T., Kim, J.Y., Kim, J.M., and Yoo, Y.H. (2004). TRAIL induces apoptosis of chondrocytes and influences the pathogenesis of experimentally induced rat osteoarthritis. Arthritis Rheum. *50*, 534–542.

Li, Y., Xu, L., and Olsen, B.R. (2007). Lessons from genetic forms of osteoarthritis for the pathogenesis of the disease. Osteoarthritis Cartilage *15*, 1101–1105.

Little, C.B., Meeker, C.T., Golub, S.B., Lawlor, K.E., Farmer, P.J., Smith, S.M., and Fosang, A.J. (2007). Blocking aggrecanase cleavage in the aggrecan interglobular domain abrogates cartilage erosion and promotes cartilage repair. J. Clin. Invest. *117*, 1627–1636.

Lorenz, H., Wenz, W., Ivancic, M., Steck, E., and Richter, W. (2005). Early and stable upregulation of collagen type II, collagen type I and YKL40 expression levels in cartilage during early experimental osteoarthritis occurs independent of joint location and histological grading. Arthritis Res. Ther. *7*, R156–165.

Manabe, N., Oda, H., Nakamura, K., Kuga, Y., Uchida, S., and Kawaguchi, H. (1999). Involvement of fibroblast growth factor-2 in joint destruction of rheumatoid arthritis patients. Rheumatology (Oxford). *38*, 714–720.

Matyas, J.R., Ehlers, P.F., Huang, D., and Adams, M.E. (1999). The early molecular natural history of experimental osteoarthritis. I. Progressive discoordinate expression of aggrecan and type II procollagen messenger RNA in the articular cartilage of adult animals. Arthritis Rheum. *42*, 993–1002.

Matyas, J.R., Huang, D., Chung, M., and Adams, M.E. (2002). Regional quantification of cartilage type II collagen and aggrecan messenger RNA in joints with early experimental osteoarthritis. Arthritis Rheum. *46*, 1536–1543.

Nagase, H., Visse, R., and Murphy, G. (2006). Structure and function of matrix metalloproteinases and TIMPs. Cardiovasc. Res. *69*, 562-573.

Okawa. A., Nakamura, I., Goto, S., Moriya, H., Nakamura, Y., and Ikegawa, S. (1998). Mutation in Npps in a mouse model of ossification of the posterior longitudinal ligament of the spine. Nat. Genet. *19*, 271–273.

Pettersen, I., Figenschau, Y., Olsen, E., Bakkelund, W., Smedsröd, B., and Sveinbjörnsson, B. (2002). Tumor necrosis factor-related apoptosis-inducing ligand induces apoptosis in human articular chondrocytes *in vitro*. Biochem. Biophys.

Res. Commun. *296*, 671–676.

Pond, M.J. and Nuki, G. (1973). Experimentally-induced osteoarthritis in the dog. Ann. Rheum. Dis. *32*, 387–388.

Sharma, L. and Kapoor, D. (2007). Epidemiology of osteoarthritis. In, Moskowitz R.W. Altman R.D. Hochberg M.C. Buckwalter J.A. Goldberg V.M. editors. In Osteoarthritis, Diagnosis and Medical/ Surgical Management. 4th ed., R.W. Moskowitz, R.D. Altman, M.C. Hochberg, J.A. Buckwalter, and V.M. Goldberg, eds. (Philadelphia, USA: Lippincott Williams & Wilkins), pp. 3–26.

Shimizu, S., Asou, Y., Itoh, S., Chung, U.I., Kawaguchi, H., Shinomiya, K., and Muneta, T. (2007). Prevention of cartilage degradation with intraarticular osteoclastogenesis inhibitory factor/osteoprotegerin in a murine model of osteoarthritis. Arthritis Rheum. *56*, 3358–3365.

Stanton, H., Rogerson, F.M., East, C.J., Golub, S.B., Lawlor, K.E., Meeker, C.T., Little, C.B., Last, K., Farmer, P.J., Campbell, I.K., et al. (2005). ADAMTS5 is the major aggrecanase in mouse cartilage *in vivo* and *in vitro*. Nature *434*, 648–652.

Takeda, S., Bonnamy, J.P., Owen, M.J., Ducy, P., and Karsenty, G. (2001). Continuous expression of Cbfa1 in nonhypertrophic chondrocytes uncovers its ability to induce hypertrophic chondrocyte differentiation and partially rescues Cbfa1-deficient mice. Genes Dev. *15*, 467–481.

Ueta, C., Iwamoto, M., Kanatani, N., Yoshida, C., Liu, Y., Enomoto-Iwamoto, M., Ohmori, T, Enomoto, H., Nakata, K., Takada, K., et al. (2001). Skeletal malformations caused by overexpression of Cbfa1 or its dominant negative form in chondrocytes. J. Cell Biol. *153*, 87–100.

Vincenti, M.P. and Brinckerhoff, C.E. (2002). Transcriptional regulation of collagenase (MMP-1. MMP-13) genes in arthritis, integration of complex signaling pathways for the recruitment of gene-specific transcription factors. Arthritis Res. *4*, 157–164.

von der Mark, K., Kirsch, T., Nerlich, A., Kuss, A., Weseloh, G., Gluckert, K., and Stöss, H. (1992). Type X collagen synthesis in human osteoarthritic cartilage. Indication of chondrocyte hypertrophy. Arthritis Rheum. *35*, 806–811.

Xu, L., Peng, H., Wu, D., Hu, K., Goldring, M.B., Olsen, B.R., and Li, Y. (2005). Activation of the discoidin domain receptor 2 induces expression of matrix metalloproteinase 13 associated with osteoarthritis in mice. J. Biol. Chem. *280*, 548–555.

Xu, L., Peng, H., Glasson, S., Lee, P.L., Hu, K., Ijiri, K., Olsen, B.R., Goldring, M.B., and Li, Y. (2007). Increased expression of the collagen receptor discoidin domain receptor 2 in articular cartilage as a key event in the pathogenesis of osteoarthritis. Arthritis Rheum. *56*, 2663–2673.

Yamada, T., Kawano, H., Koshizuka, Y., Fukuda, T., Yoshimura, K., Kamekura, S., Saito, T., Ikeda, T., Kawasaki, Y., Azuma, Y., et al. (2006). Carminerin contributes to chondrocyte calcification during endochondral ossification. Nat. Med. *12*, 665–670.

Yamakawa, K., Kamekura, S., Kawamura, N., Saegusa, M., Kamei, D., Murakami, M., Kudo, I., Uematsu, S., Akira, S., Chung, U.I., et al. (2008). Association of microsomal prostaglandin E synthase 1 deficiency with impaired fracture healing, but not with bone loss or osteoarthritis, in mouse models of skeletal disorders. Arthritis Rheum. *58*, 172–183.

ARTHRITIS & RHEUMATISM
Vol. 58, No. 1, January 2008, pp 172–183
DOI 10.1002/art.23158

Association of Microsomal Prostaglandin E Synthase 1 Deficiency With Impaired Fracture Healing, But Not With Bone Loss or Osteoarthritis, in Mouse Models of Skeletal Disorders

Kiyofumi Yamakawa,[1] Satoru Kamekura,[1] Naohiro Kawamura,[1] Masatomo Saegusa,[1] Daisuke Kamei,[2] Makoto Murakami,[3] Ichiro Kudo,[2] Satoshi Uematsu,[4] Shizuo Akira,[4] Ung-il Chung,[1] Kozo Nakamura,[1] and Hiroshi Kawaguchi[1]

Objective. **Prostaglandin E synthase (PGES) functions as the terminal enzyme in the biosynthesis of prostaglandin E_2 (PGE_2) and is a potent regulator of bone and cartilage metabolism. Among the 3 isozymes of PGES, microsomal PGES-1 (mPGES-1) is known to play the most critical role in the production of PGE_2 in pathophysiologic events. This study investigated the roles of mPGES-1 under normal physiologic and pathophysiologic conditions in the skeletons of mPGES-1–deficient ($mPGES\text{-}1^{-/-}$) mice.**

Methods. **Skeletons of $mPGES\text{-}1^{-/-}$ mice and their wild-type littermates were compared by radiologic and histologic analyses. Four models of skeletal disorders were created: bone loss induced by ovariectomy, bone loss induced by hind limb unloading, osteoarthritis (OA) induced by instability in the knee joint, and bone fracture by osteotomy at the tibial midshaft. Expression of the PGES enzymes was examined by immunohistochemistry and real-time reverse transcription–polymerase chain reaction. The cellular mechanism of fracture healing was examined in ex vivo cultures of costal cartilage chondrocytes.**

Results. **Microsomal $PGES\text{-}1^{-/-}$ mice had unaffected skeletal phenotypes under normal physiologic conditions. In the bone fracture model, fracture healing was impaired by the mPGES-1 deficiency, with half of the mice remaining in a non–bone union state even after 21 days; normal fracture healing was restored by adenoviral reintroduction of mPGES-1. The other skeletal disorders were not affected by the mPGES-1 deficiency. In vivo and ex vivo analyses revealed an impaired proliferation of chondrocytes in cartilage with the mPGES-1 deficiency, at an early stage of fracture healing.**

Conclusion. **In these mouse models of skeletal disorders, mPGES-1 was indispensable for bone repair through chondrocyte proliferation, but was not essential for the skeleton under normal physiologic conditions, nor did it play a role in the pathophysiologic conditions of bone loss due to ovariectomy, bone loss due to unloading, or stress-induced OA.**

Prostaglandin E_2 (PGE_2) is produced in many types of tissue, including bone and cartilage, and has a broad range of biologic activities that are carried out via binding to 4 different G protein–coupled receptors, EP1, EP2, EP3, and EP4, which are linked to different intracellular signaling pathways (1,2). In the biosynthesis of PGE_2, 3 enzymatic steps have been identified, involving phospholipase A_2, cyclooxygenase (COX), and prostaglandin E synthase (PGES).

PGES, the terminal enzyme that catalyzes the conversion of PGH_2 to PGE_2, exists as 2 membrane-associated enzymes, microsomal PGES-1 (mPGES-1)

Supported by a Grant-in-Aid for Scientific Research from the Japanese Ministry of Education, Culture, Sports, Science, and Technology (14370452).

[1]Kiyofumi Yamakawa, MD, PhD, Satoru Kamekura, MD, PhD, Naohiro Kawamura, MD, Masatomo Saegusa, MD, PhD, Ung-il Chung, MD, PhD, Kozo Nakamura, MD, PhD, Hiroshi Kawaguchi, MD, PhD: University of Tokyo, Tokyo, Japan; [2]Daisuke Kamei, PhD, Ichiro Kudo, PhD: Showa University, Tokyo, Japan; [3]Makoto Murakami, PhD: Tokyo Metropolitan Institute of Medical Science, Tokyo, Japan; [4]Satoshi Uematsu, MD, PhD, Shizuo Akira, MD, PhD: Osaka University, Osaka, Japan.

Address correspondence and reprint requests to Hiroshi Kawaguchi, MD, PhD, Sensory and Motor System Medicine, Faculty of Medicine, University of Tokyo, Hongo 7-3-1, Bunkyo, Tokyo 113-8655, Japan. E-mail: kawaguchi-ort@h.u-tokyo.ac.jp.

Submitted for publication March 5, 2007; accepted in revised form September 21, 2007.

and mPGES-2, and 1 cytosolic enzyme, cPGES (3–9). Microsomal PGES-1 is a glutathione (GSH)–requiring perinuclear protein that belongs to the family of MAPEGs (membrane-associated proteins involved in eicosanoid and GSH metabolism), is induced by proinflammatory stimuli and suppressed by glucocorticoids, and is functionally coupled with COX-2 in marked preference to COX-1 (4,5). Induction of mPGES-1 expression is observed in various conditions in which COX-2–derived PGE_2 plays a critical role, such as inflammation, tissue repair, fever, pain, dysfunctioning of the female reproductive system, cancer, and bone resorption (3,10). In contrast, mPGES-2, which has a catalytic glutaredoxin- or thioredoxin-like domain, is constitutively expressed in various tissues and functionally coupled with both COX-1 and COX-2 (8,9). Cytosolic PGES, also constitutively expressed in a wide variety of cells, is functionally linked to COX-1, but not to COX-2, to promote immediate PGE_2 production (11,12).

Among the PGES enzymes, biochemical and biologic analyses have led to the proposal that mPGES-1 plays the most critical role in the production of PGE_2 in various pathophysiologic events. An initial study with mPGES-1–knockout (mPGES-$1^{-/-}$) mice revealed the essential role of mPGES-1 in lipopolysaccharide (LPS)–stimulated PGE_2 production by macrophages, although the mice remained fertile and developed and grew normally (13). Further analyses of mPGES-$1^{-/-}$ mice, performed by us and by other investigators, have shown an important role of mPGES-1 in pain sensitivity, febrile responses, and tissue granulation accompanying angiogenesis (14,15).

In bone, PGE_2 is the most abundant prostanoid and strongly regulates both bone resorption and bone formation (1). We previously reported that mPGES-1 is induced by bone-resorptive cytokines, preceded by the induction of COX-2, in osteoblasts, and that the induction of mPGES-1 mediates the catabolic effects of the osteoblasts (10). Similar to mice deficient in COX-2 and EP4 (2,16), mPGES-$1^{-/-}$ mice were shown to be resistant to LPS-induced bone resorption (17).

PGE_2 is also known to be a potent stimulator of bone formation (1), so that selective agonists of EP2 and EP4 stimulate bone formation (2,18). Although recent studies of PGE_2 receptor–knockout or COX-2–knockout mice failed to demonstrate abnormalities in skeletal development or growth, bone formation was impaired by the deficiency under pathologic conditions (2,19,20).

PGE_2 is also known to have a role in both catabolic and anabolic regulation of chondrocyte functions (21). In joint cartilage, it acts as one of the major catabolic mediators involved in cartilage degradation (22–24). Studies of knockout mice revealed the contributory roles of mPGES-1 and EP4 to collagen-induced arthritis (CIA) (14,15,25). In addition, PGE_2 is produced more abundantly in osteoarthritic (OA) cartilage than in normal cartilage (26), and mPGES-1 is a key enzyme in the regulation of PGE_2 production in chondrocytes from patients with OA (27). Thus, the present study investigated the contribution of mPGES-1 to bone and cartilage metabolism under normal physiologic and pathophysiologic conditions, by creating models of ovariectomy- or hind limb unloading–induced bone loss, joint instability–induced OA, and bone fracture in mPGES-$1^{-/-}$ mice.

MATERIALS AND METHODS

Animals. The generation of mPGES-1 gene–targeted mice has been described previously (13). In each experiment, mPGES-$1^{-/-}$ mice and their wild-type (WT) littermates were fed a standard diet. All experiments were performed according to the protocol approved by the Animal Care and Use Committee of the University of Tokyo.

Bone morphology. A bone radiograph of the whole bodies, femurs, and tibias was obtained with a soft x-ray apparatus (CMB-2; Softex, Tokyo, Japan). The bone mineral density (BMD; mg/cm^2) of the right femurs, tibias, and L2–L5 vertebral bodies was determined using dual x-ray absorptiometry (DXA) (PIXImus; Lunar, Madison, WI), according to the manufacturer's instructions. Histologic analyses were carried out on the left tibias of 8-week-old mice. For assessment of dynamic histomorphometric indices, mice were injected subcutaneously with 16 mg/kg body weight of calcein, at 10 days and 3 days before termination. Thereafter, the tibias were excised and fixed with ethanol, and the undecalcified bones were embedded in methyl methacrylate.

Six-micrometer frontal sections from the proximal parts of the tibias were stained with Villanueva-Goldner, and were visualized under light fluorescence microscopy for calcein labeling. Growth plates were stained with toluidine blue. Tartrate-resistant acid phosphatase–positive cells were stained at pH 5.0 in the presence of L(+)-tartaric acid, using naphthol-AS-MX phosphate in *N,N*-dimethylformamide as the substrate. The specimens were subjected to histomorphometric analyses using a semiautomated system (Osteoplan II; Carl Zeiss Instruments, Thornwood, NY). Parameters for the trabecular bone were measured in an area 1.2 mm in length to a depth 0.3 mm below the growth plate at the proximal metaphysis of the tibias.

Ovariectomy experiment. Twenty-six-week-old female mPGES-$1^{-/-}$ and WT mice underwent a bilateral ovariectomy or a sham operation under general anesthesia, as we have previously reported (28). Mice were killed 4 weeks after the surgery, and the weight of the excised uterus was measured. The BMD of the tibias was measured by DXA immediately

before the surgery and 4 weeks after surgery. Results for each mouse were calculated as the percent loss of BMD during that period.

Tail suspension experiment. Eight-week-old female mPGES-1$^{-/-}$ and WT mice were subjected to tail suspension for 4 weeks. A tape was applied to the surface of the tail for placement of a metal clip. The end of the clip was fixed to an overhead bar and the position of the tape was adjusted to maintain the mice in a 30° head-down tilt with the hind limbs elevated above the floor of the cage. For the control group, mice were housed individually under the same conditions but were not subjected to tail suspension, so that the hind limbs remained in a weight-bearing position (loaded control). After 4 weeks, the mice were killed and the right tibias were subjected to BMD measurement and histomorphometric analysis.

OA experiment. The surgical procedure to create an OA experimental model was performed on 8-week-old male mice, as we have reported previously (29–31). Briefly, mice were placed under general anesthesia and the medial collateral ligament was transected. The medial meniscus was then removed using a surgical microscope. Fourteen weeks after surgery, the mice were killed and the entire knee joints were dissected, decalcified, and stained with Safranin O–fast green. Destruction of cartilage was quantified as the most severe changes among 20 serial sections according to our original histologic grading scale of 0–4 (29), which was assessed by a single observer (SK) who was blinded to the experimental group.

Fracture experiment. A transverse osteotomy at the midshaft of the right tibia was created at the midshaft using a bone saw, and was internally stabilized with an intramedullary nail using the inner pin of a spinal needle of 22- or 23-gauge diameter, depending on the size of the cavity, as we have reported previously (30,32). The left tibia (unfractured side) was subjected to sham operation and an intramedullary nail of the same size was inserted. To determine whether there was bone union, bony bridging on radiographs was evaluated by a single observer (SK) who was blinded to the experimental group. The area and bone mineral content (BMC) of the entire tibia were measured bilaterally using DXA. The area and BMC of the tibias were measured bilaterally before and at various time points after the fracture operation, and differences in the increased values (gain of area and percent gain of BMC) between the right (fractured) tibia and left (unfractured) tibia were calculated.

For histologic analyses, specimens of the harvested tibias were fixed with 4% paraformaldehyde, decalcified with EDTA, dehydrated with ethanol, embedded in paraffin, and cut into 4-μm sections. The sections were stained with hematoxylin and eosin or toluidine blue. For immunohistochemistry, samples were examined in dewaxed paraffin–embedded sections. After dehydration, the sections were treated with 0.3% hydrogen peroxide and then with 1% bovine serum albumin, and incubated with a polyclonal rabbit antibody to mPGES-1 (Cayman Chemical, Ann Arbor, MI) or type X collagen (COL10; Santa Cruz Biotechnology, Santa Cruz, CA) at a dilution of 1:100. The sections were then incubated with horseradish peroxidase–conjugated goat antibody against rabbit IgG (Dakopatts, Glostrup, Denmark).

For bromodeoxyuridine (BrdU) labeling, mice were injected intraperitoneally with BrdU (25 μg/gram body weight) 2 hours prior to termination. Incorporated BrdU was detected using a BrdU staining kit (Zymed, San Francisco, CA). TUNEL staining was performed using an Apoptosis in Situ Detection kit (Wako Pure Chemical, Osaka, Japan) according to the manufacturer's instructions.

For measurement of PG levels, fracture callus and sham-operated sites of the tibias were homogenized 7 days after surgery in a homogenization buffer containing 10 μM indomethacin. Aliquots were then adjusted to pH 3.0 with 1N HCl and passed through Sep-Pak C18 cartridges (Cayman Chemical), and the retained PGs were eluted from the cartridges with methanol. A trace amount of ^{3}H-PGE$_2$ (Cayman Chemical) was added to the samples before passage through the cartridges, to calibrate the recovery of PGs. The solvent of the samples was evaporated, and the PGs were dissolved in an aliquot of buffer and assayed with PGE$_2$ and PGF$_{2\alpha}$ enzyme immunoassay kits (Cayman Chemical) according to the manufacturer's instructions.

Real-time reverse transcription–polymerase chain reaction (RT-PCR) analysis. Total RNA was extracted from the fracture callus by isogen–chloroform extraction and isopropanol precipitation (Nippon Gene, Tokyo, Japan), according to the manufacturer's instructions. Total messenger RNA (mRNA) (1 μg) was reverse transcribed using Superscript reverse transcriptase with random hexamer (Takara Shuzo, Shiga, Japan), and 1 μl of each reverse transcriptase reaction was used as a template for the second-step SYBR Green real-time RT-PCR. The full-length or partial-length complementary DNA of target genes, including PCR amplicon sequences, was amplified by PCR, cloned into pCR4-TOPO vectors (Invitrogen, Carlsbad, CA), and used as standard templates after linearization. QuantiTect SYBR Green PCR Master Mix (Qiagen, Chatsworth, CA) was used for the second-step SYBR Green real-time RT-PCR, according to the manufacturer's instructions. SYBR Green PCR amplification and real-time fluorescence detection were performed using an ABI Prism 7700 sequence detection system (Applied Biosystems, Foster City, CA). All reactions were run in quadruplicate.

Copy numbers of target gene mRNA in each total RNA were calculated by reference to standard curves and were adjusted to the mouse standard total RNA (Applied Biosystems) with the mouse actin as an internal control. PCR amplification was performed using the following specific primer pairs: for mPGES-1, sense 5′-TTACAGGAGTGACCCAGATGT-3′ and antisense 5′-GAGAACTGGGCCAGGACATA-3′; for mPGES-2, sense 5′-ACATCCAGCCTTGGTACCTG-3′ and antisense 5′-TGTAAGTTTGGGCCTTGTCC-3′; for cPGES, sense 5′-CGATCCAAATGATTCCAAGC-3′ and antisense 5′-CATCCTCCCAGTCTTTCCAA-3′; and for actin, sense 5′-AGATGTGGATCAGCAAGCAG-3′ and antisense 5′-GCGCAAGTTAGGTTTTGTCA-3′.

Isolation and culture of mouse costal chondrocytes. Newborn mice were killed and the costal cartilage, not including the soft tissue, was digested with 0.3% collagenase in Dulbecco's modified Eagle's medium (DMEM) (Sigma, St. Louis, MO) at 37°C for 5 hours. For the cell proliferation assay, primary chondrocytes from mPGES-1$^{-/-}$ and WT mice were incubated at a density of 5,000 cells/well in DMEM with

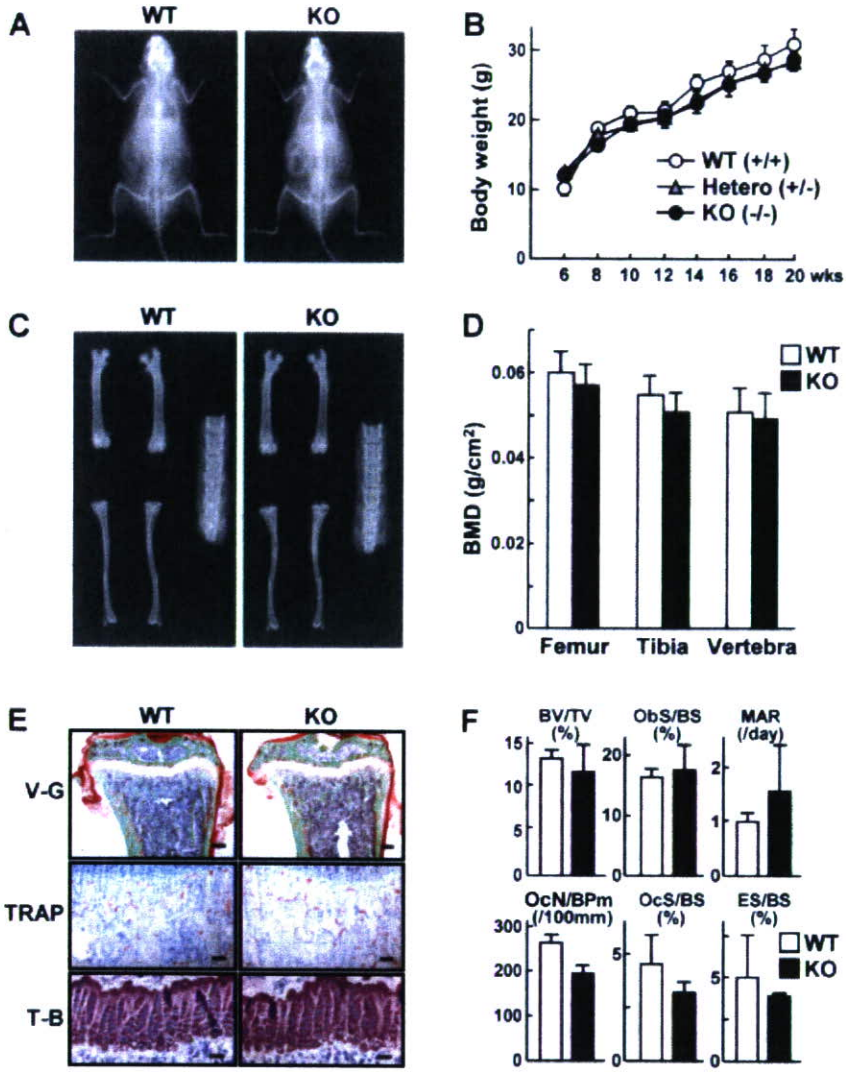

Figure 1. Radiologic and histologic findings in the bones of microsomal prostaglandin E synthase 1–knockout (KO) (mPGES-1$^{-/-}$) mice and their wild-type (WT) littermates under normal physiologic conditions. **A,** Radiologic images of the whole body of representative 8-week-old male WT and KO mice. **B,** Growth curves, as determined by body weight, of the male WT, mPGES-1$^{+/-}$, and mPGES-1$^{-/-}$ mice. Results are the mean ± SEM of 20 mice/group. **C,** Radiologic images of the femurs, tibias, and lumbar vertebrae of representative 8-week-old male WT and KO mice. **D,** Bone mineral density (BMD) of the entire femurs, tibias, and L2–L5 vertebrae, as determined by dual x-ray absorptiometry. Bars show the mean and SEM of 8 bones/group. **E,** Histologic features of the proximal tibias of WT and KO mice. With Villanueva-Goldner (V-G) staining, mineralized bone is stained green and unmineralized osteoid is stained red (bar = 200 μm). With tartrate-resistant acid phosphatase (TRAP) staining of the primary spongiosa below the growth plate, osteoclasts are stained red (bar = 50 μm). With toluidine blue (T-B) staining of the growth plate, cartilage matrix is stained purple (bar = 20 μm). **F,** Histomorphometric parameters in the proximal tibias of WT and KO mice. Bars show the mean and SEM of 3 mice/group. BV/TV = bone volume per total volume; ObS/BS = osteoblast surface per bone surface; MAR = mineral apposition rate; OcN/BPm = number of osteoclasts per 100 mm of bone perimeter; OcS/BS = osteoclast surface per bone surface; ES/BS = eroded surface per bone surface.

10% fetal bovine serum. The number of cells/well was counted using a WST-8 assay with a Cell Counting Kit 8 (Dojindo, Kumamoto, Japan), with results expressed as the absorbance of each well at 450 nm. For alkaline phosphatase staining, performed on day 14 after confluency, cultured cells were fixed in 70% ethanol and stained for 10 minutes with a solution containing 0.01% naphthol-AS-MX phosphate disodium salt (Sigma), 1% *N,N*-dimethylformamide (Wako Pure Chemical), and 0.06% Fast Blue BB. For alizarin red S staining, performed on day 21 after confluency, cells were fixed in 10% buffered

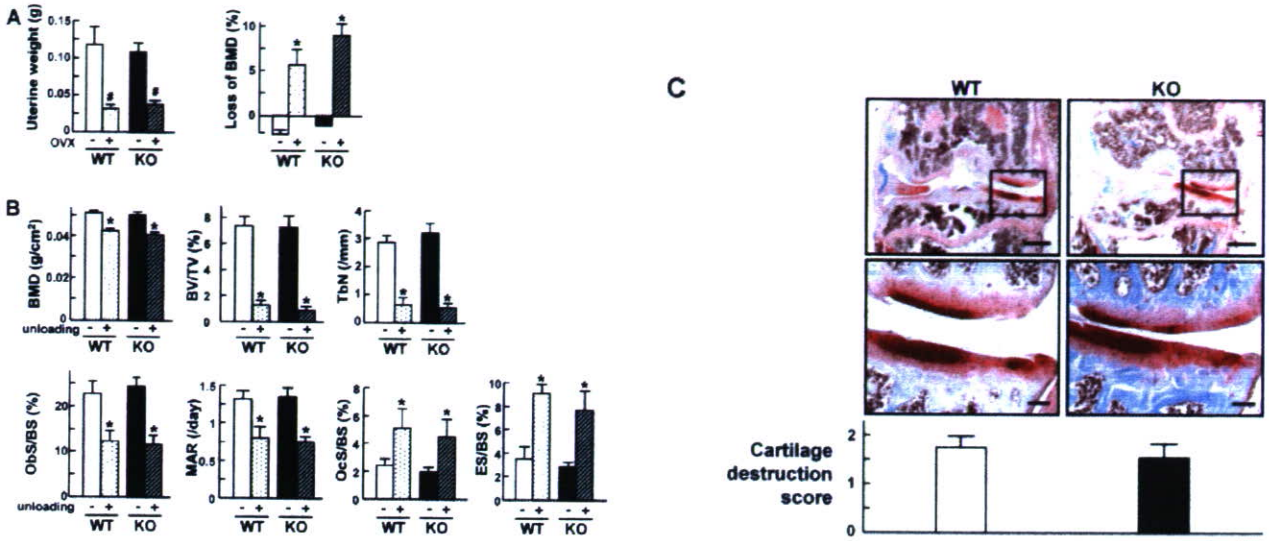

Figure 2. **A,** Effects of ovariectomy (OVX) on the bones of KO (mPGES-1$^{-/-}$) mice and their WT littermates. Female mice underwent ovariectomy (+) or sham operation (−) at age 26 weeks, and were killed at 30 weeks. Values for uterus weight at 30 weeks (left) and percentage loss of BMD of the tibia at 4 weeks after surgery (right) are the mean and SEM of 5 mice/group. There were no significant differences between the WT and mPGES-1$^{-/-}$ mice. # = $P < 0.05$; * = $P < 0.01$, versus sham-operated mice. **B,** Effects of unloading of the proximal tibias (+) of WT and mPGES-1$^{-/-}$ mice. Unloading was performed using the tail suspension model in 8-week-old female littermates, and BMD and histomorphometric parameters were assessed at 4 weeks after unloading. BMD results are the mean and SEM of 8 mice/group, while histomorphometric parameters (BV/TV, trabecular number [TbN], ObS/BS, MAR, OcS/BS, and ES/BS) are the mean and SEM of 3 mice/group. There were no significant differences between the WT and mPGES-1$^{-/-}$ mice. * = $P < 0.01$ versus loaded (−) controls. **C,** Cartilage destruction in the medial portion of the tibial cartilage during the development of osteoarthritis induced by knee joint instability. Eight-week-old male WT and mPGES$^{-/-}$ mice underwent medial collateral ligament transection and medial meniscus resection of the right knee joint. Shown are representative results from Safranin O staining of the frontal sections of the knee (top and middle) and histologic scoring of cartilage destruction (mean and SEM of 3 mice/group) (bottom) at 14 weeks after surgery. Boxed areas in the top panels are shown in higher magnification in the middle panels (top, bar = 500 μm; middle, bar = 50 μm). See Figure 1 for other definitions.

formalin and stained for 10 minutes with 2% alizarin red S (pH 4.0).

Generation of adenoviruses and gene transfer. The recombinant adenovirus vectors carrying the mPGES-1 gene (Ax-mPGES-1) and the control β-galactosidase gene (Ax-LacZ) that was engineered to express the hemagglutinin tag at its N-terminus were constructed using the Adenoviral Expression System (Invitrogen), following the manufacturer's protocol. Two days after the operation, a suspension of 10^{12} plaque-forming units of Ax-mPGES-1 or Ax-LacZ was injected into the fracture site, as described previously (33). Animals were killed 14 days after the injection, with subsequent analyses carried out as described above.

Statistical analysis. The mean values of each group were compared by analysis of variance. Significant differences between groups were determined by post hoc testing with Bonferroni's method.

RESULTS

Skeletal phenotypes of mPGES-1$^{-/-}$ mice under normal physiologic conditions. We initially analyzed the skeletons of mPGES-1$^{-/-}$ mice under normal physiologic conditions. Radiologic analyses showed no significant differences in the skeleton between mPGES-1$^{-/-}$ mice and their WT littermates (Figure 1A). The mPGES-1$^{-/-}$ mice grew normally and had no abnormalities in the major organs. Moreover, growth curves, as determined by body weight, were similar among the WT, mPGES-1$^{+/-}$, and mPGES-1$^{-/-}$ mice during an observation period of up to 20 weeks of age (Figure 1B).

The BMDs of the femurs, tibias, and lumbar vertebrae were also comparable between mPGES-1$^{-/-}$ mice and their WT littermates (Figures 1C and D). Furthermore, histologic analyses revealed no differences between groups in the bone volume or osteoclast number (Figure 1E), and these findings were supported by histomorphometric measurements that showed comparable values for bone volume (assessed as bone volume per total volume), bone formation parameters (osteoblast surface per bone surface, and mineral apposition rate), and bone resorption parameters (number of osteoclasts per 100 mm of bone perimeter, osteoclast surface

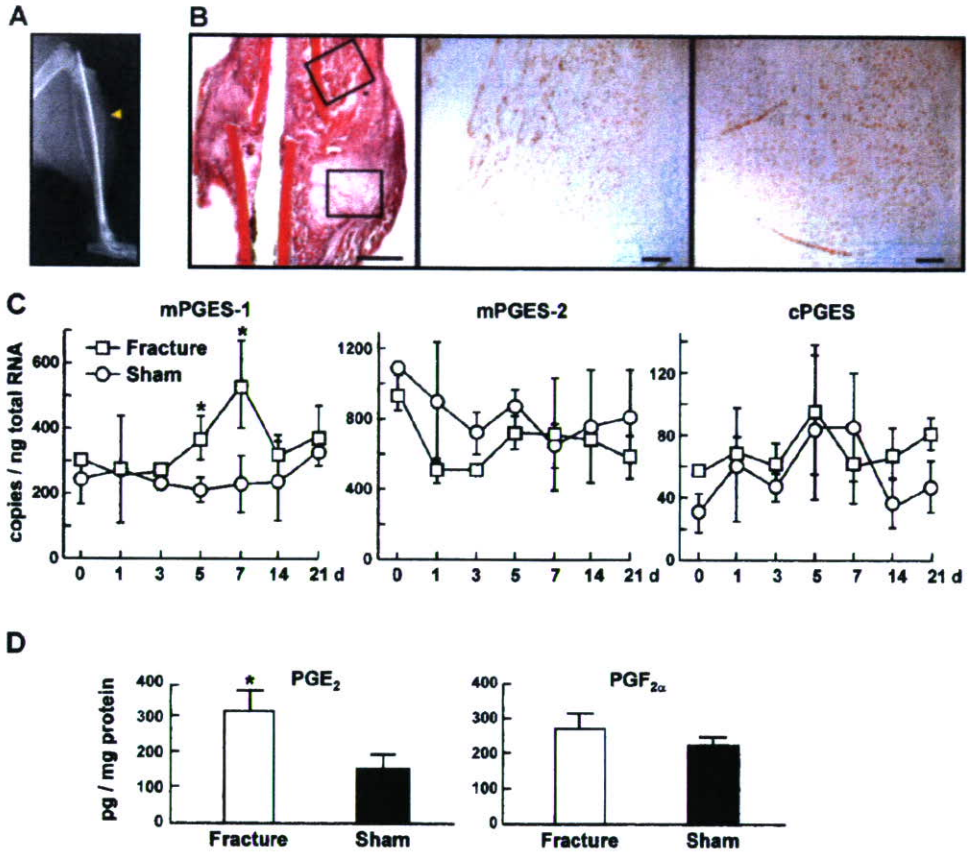

Figure 3. Expression of PGES enzymes and levels of prostaglandin E_2 (PGE_2) and $PGF_{2\alpha}$ in the fracture callus of WT mice. **A,** Radiologic image of the bone fracture model in WT mice, produced by a transverse osteotomy that was stabilized with an intramedullary nail **(arrowhead)** at the midshaft of the right tibia at 8 weeks of age. **B,** Hematoxylin and eosin staining of the fracture callus 7 days after fracture (left), and immunohistochemical staining of mPGES-1 (middle and right). Boxed areas in the left panel are shown in higher magnification in the middle and right panels (left, bar = 1 mm; middle and right, bar = 100 μm). **C,** Time course (in days) of changes in mPGES-1, mPGES-2, and cytosolic PGES (cPGES) mRNA levels in the fracture callus of the right tibia and in the sham-operated site of the left tibia, determined by real-time reverse transcription–polymerase chain reaction. Bars show the mean ± SEM of 3 mice/group. * = $P < 0.05$ versus sham-operated site. **D,** PGE_2 and $PGF_{2\alpha}$ levels assessed by enzyme immunoassay in the fracture callus, as compared with the sham-operated site, at 7 days after surgery. Bars show the mean and SEM of 6 mice/group. * = $P < 0.01$ versus sham-operated site. See Figure 1 for other definitions.

per bone surface, and eroded surface per bone surface) (Figure 1F).

In addition to bone phenotypes, the height of the growth plate and the columnar architecture of chondrocytes were similar between the 2 genotypes (Figure 1E, bottom). This explains the observed lack of effect on skeletal growth, and indicates that the mPGES-1 deficiency does not affect chondrocyte function under normal physiologic conditions.

Skeletal phenotypes of mPGES-1$^{-/-}$ mice under pathophysiologic conditions. We then examined the effects of the mPGES-1 deficiency on bone phenotypes under pathophysiologic conditions. Initially, we investigated the involvement of mPGES-1 in bone loss induced by estrogen deficiency, by performing ovariectomy or sham operation on 26-week-old female mPGES-1$^{-/-}$ mice and their WT littermates. Four weeks after surgery, the change in BMD of the entire tibias of each mouse

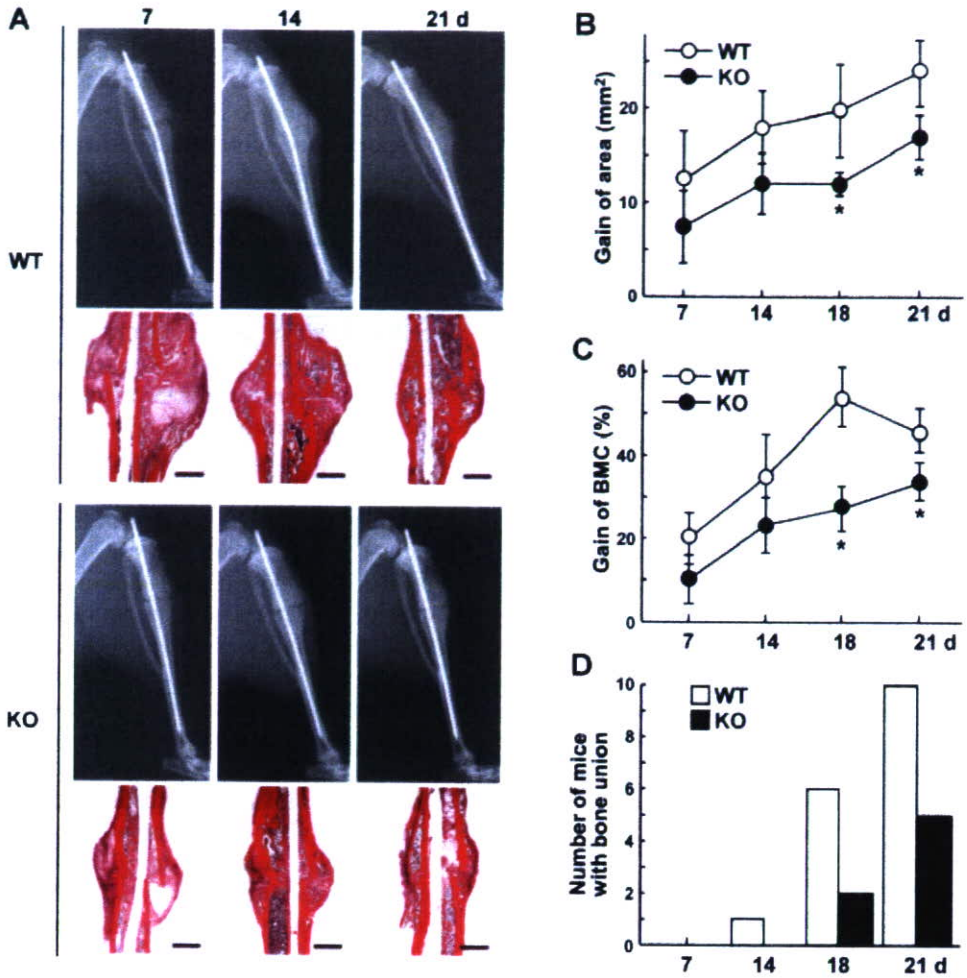

Figure 4. Bone fracture healing in KO (mPGES-1$^{-/-}$) mice and their WT littermates. **A,** Assessment by plain radiography and hematoxylin and eosin staining at 7, 14, and 21 days after fracture. Bar = 1 mm. **B** and **C,** Time course of the gain of area **(B)** and percent gain in bone mineral content (BMC) **(C)** in the fracture callus. The area and BMC of the entire tibias were measured bilaterally before and after the operation at the indicated time points (in days), and the difference between the right (fractured) and left (unfractured) tibias was calculated. Bars show the mean ± SEM of the gains as compared with the values before the operation, in 10 mice/group. * = $P < 0.05$ versus WT mice. **D,** Time course (in days) of the number of mice displaying bone union among 10 mice/group, determined by radiographic assessment of complete bony bridging at the fracture site. See Figure 1 for other definitions.

was compared between genotypes. The weight of the uterus was confirmed to be decreased by ovariectomy in both genotypes (Figure 2A). Similarly, the BMD was also decreased in both groups (Figure 2A), indicating that mPGES-1 does not contribute to bone loss caused by estrogen deficiency.

We then studied the role of this enzyme in bone loss induced by unloading, using the tail suspension model. Four weeks after tail suspension, radiologic and histologic analyses of the tibias were performed. Similar to the findings described above, both genotypes showed comparable decreases in BMD after hind limb unloading, as compared with the values in the loaded controls (Figure 2B). Histomorphometric analyses revealed that bone formation parameters were decreased, while bone resorption parameters were increased, by hind limb unloading, and that these changes were not affected by the mPGES-1 deficiency, which indicates that this enzyme is not essential for unloading-induced bone loss.

We then compared the susceptibility to OA in-

duced by knee joint instability between mPGES-$1^{-/-}$ and WT mice (Figure 2C), with cartilage destruction assessed using our original model and grading scheme (29). Safranin O staining showed that cartilage destruction progressed into the middle zone of the medial cartilage by 14 weeks after surgery, and this was evident in both genotypes. Quantification of cartilage destruction by our original grading system confirmed that the mPGES-1 deficiency does not affect OA induced by joint instability.

Expression of PGES enzymes and prostanoids in the fracture callus. To understand the involvement of PGES enzymes and PGE_2 in bone fracture healing, we created a fracture at the midshaft of the tibia in WT mice (Figure 3A) and examined the expression of mPGES-1, mPGES-2, and cPGES. Immunolocalization of mPGES-1 was visible 7 days after the fracture, in areas of both intramembranous and endochondral bone formation (Figure 3B). Among the 3 enzymes, only the mPGES-1 mRNA level increased, at 5 and 7 days after surgery, at the fracture callus of the right tibia, as compared with the sham-operated site of the left tibia (Figure 3C). In addition, the level of PGE_2 was confirmed to be higher at the callus 7 days after surgery, while the $PGF_{2\alpha}$ level at the fracture callus was comparable with that at the sham-operated site (Figure 3D).

Bone fracture healing in mPGES-$1^{-/-}$ mice. We then used the same fracture model as described above to compare the healing process in mPGES-$1^{-/-}$ and WT mice at 8 weeks of age and examine the effect of the mPGES-1 deficiency. In WT mice, a large soft callus had formed by 7 days after fracture and was thereafter reduced in size during ossification. Bony bridging was complete within 14–21 days (Figure 4A, top). In mPGES-$1^{-/-}$ mice, however, the size of the callus was smaller at 7 days after fracture, and fibrous tissue still remained in the fracture gap even at 21 days, indicative of a state of non–bone union (Figure 4A, bottom).

Evaluation of the time course of the gain of area (Figure 4B) and gain of BMC (Figure 4C) of the fracture callus revealed that, starting 7 days after fracture, impairment of callus formation became evident in mice with the mPGES-1 deficiency, with significant differences compared with WT mice by 18 days and thereafter. Determination of the number of mice with radiologic bone union revealed that 5 mPGES-$1^{-/-}$ mice remained in a non–bone union state even at 21 days after fracture, at which time all WT mice had achieved bone union (Figure 4D). Taken together, these findings reveal that the mPGES-1 deficiency probably caused an impairment of fracture healing from the early stage, when the required amount of soft callus must be formed.

Mechanism of impaired fracture healing by mPGES-1 deficiency. To examine the mechanism underlying the impaired fracture healing that occurs at an early stage and is attributable to mPGES-1 deficiency, we performed more detailed histologic analyses of the fracture callus at 7 days after surgery (Figure 5A). Toluidine blue staining revealed a decrease in the size of the soft callus in mPGES-$1^{-/-}$ mice, especially in the cartilaginous tissue. Moreover, in the tissue, BrdU-positive proliferative cells were abundant in the fracture callus of WT mice but were hardly detectable in that of the mPGES-$1^{-/-}$ mice, indicating that chondrocyte proliferation was markedly impaired by the mPGES-1 deficiency. In contrast, COL10 immunostaining and TUNEL staining, representing hypertrophic and apoptotic chondrocytes, were normally visible in the cartilaginous area of the callus of mPGES-$1^{-/-}$ mice, although the areas of positive staining were somewhat smaller than those in the callus of the WT mice, implying that these defects may be secondary to the impaired proliferation of mPGES-$1^{-/-}$ chondrocytes.

We then compared the functions of cultured chondrocytes isolated from WT and mPGES-$1^{-/-}$ costal cartilage. The growth curve at 7 days after seeding confirmed that the chondrocytes from mPGES-$1^{-/-}$ mice had impaired mitogenic ability. The number of cells in mPGES-$1^{-/-}$ mice was significantly lower than that in WT mice at 5 days and thereafter (Figure 5B). In contrast, chondrocyte differentiation, as determined by alkaline phosphatase and alizarin red staining, was similar between the 2 genotypes (Figure 5C). Thus, the impairment of bone fracture healing by the mPGES-1 deficiency may be due to a decrease in the mitogenic ability of chondrocytes, but not due to a decrease in the differentiation or survival of chondrocytes.

Finally, to determine whether the impaired healing was a tissue-autonomous effect of the mPGES-1 deficiency, we injected an adenovirus vector carrying the mPGES-1 gene (Ax-mPGES-1) or LacZ (Ax-LacZ) into the fracture site 2 days after the fracture (Figure 5D). Expression of the transgene was confirmed by X-Gal staining in and around the Ax-LacZ–injected fracture sites, as we have previously reported (32). Reintroduction of Ax-mPGES-1 into the fracture callus of mPGES-$1^{-/-}$ mice significantly restored both the area and the BMC 14 days after injection, indicating that the mPGES-1 deficiency was the cause of the impaired fracture healing, via a tissue-autonomous mechanism.

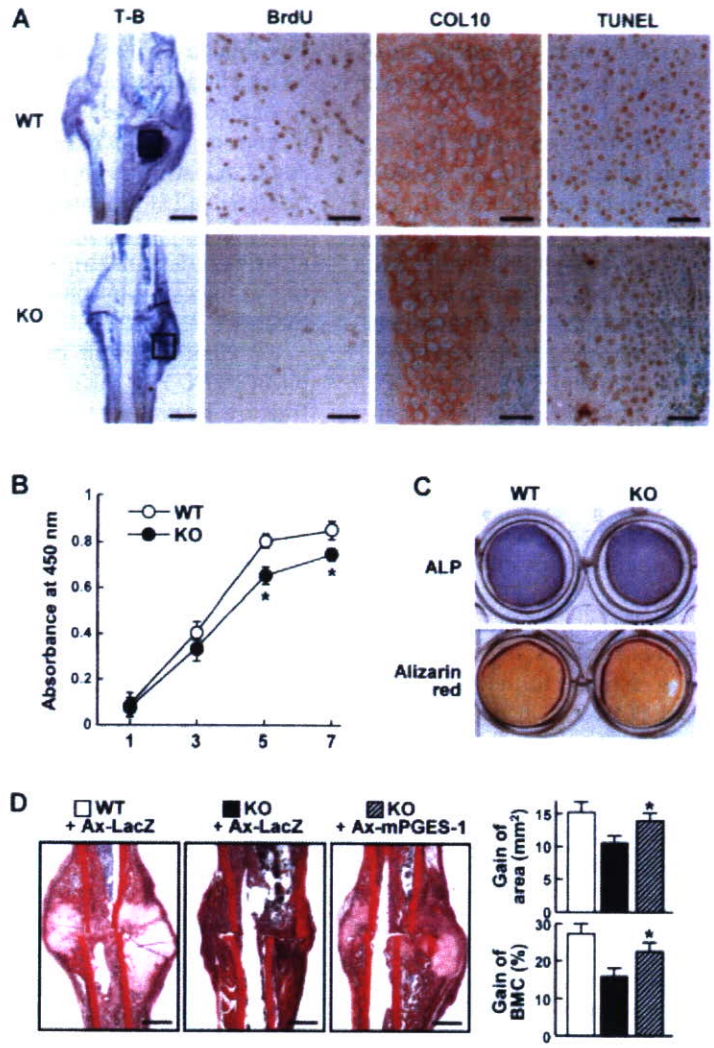

Figure 5. Mechanism of impaired fracture healing in mPGES-$1^{-/-}$ mice. **A,** Histologic and immunohistochemical findings in the fracture callus in WT and mPGES-$1^{-/-}$ mice 7 days after the fracture, using toluidine blue (T-B) staining, bromodeoxyuridine (BrdU) labeling, type X collagen (COL10) immunohistochemical staining, and TUNEL staining. Boxed areas in the T-B images are shown in higher magnification in the other images (T-B, bar = 1 mm; BrdU, COL10, and TUNEL, bar = 50 μm). **B,** Growth curves of cultured chondrocytes isolated from WT and mPGES-$1^{-/-}$ costal cartilage. Chondrocytes were incubated at a density of 5,000 cells/well in 96-multiwell plates, and the number of cells/well was determined by the absorbance at 450 nm at 7 days after seeding. Bars show the mean ± SEM of 8 wells/group. * = $P < 0.01$ versus WT mice. **C,** Differentiation of the costal chondrocytes, as determined by alkaline phosphatase (ALP) and alizarin red staining after 14 and 21 days of culture, respectively. **D,** Fracture callus formation by reintroduction of mPGES-1 using an adenoviral construct (Ax-mPGES-1) or the control LacZ (Ax-LacZ) in WT and mPGES-$1^{-/-}$ mice. Bar = 1 mm. Ax-mPGES-1 or Ax-LacZ was injected into the fracture site 2 days after surgery, and animals were killed 14 days after the injection. The gain of area and the percent gain of bone mineral content (BMC) of the fracture callus were measured as described above. Bars show the mean and SEM of 3 mice/group. * = $P < 0.05$ versus KO + Ax-LacZ. See Figure 1 for other definitions.

DISCUSSION

In accordance with the reports of previous studies indicating a lack of skeletal abnormalities in mPGES-$1^{-/-}$ mice under normal physiologic conditions (13–15), the present study confirmed this feature by detailed radiologic and histologic analyses (Figure 1). With regard to skeletal abnormalities under pathophysiologic conditions, we and others have previously reported that

mPGES-1$^{-/-}$ mice are resistant to CIA (14,15). Furthermore, another study of knockout mice showed a suppression of LPS-induced bone loss in mice with the mPGES deficiency (17).

Among the 4 skeletal disorders examined herein, only fracture healing was impaired by the mPGES-1 deficiency. This discrepancy indicates that there are differences in the contribution of mPGES-1 to these disorders, i.e., the enzyme plays an essential role in CIA, LPS-induced bone loss, and fracture healing but appears to be unnecessary for ovariectomy- or unloading-induced bone loss and OA induced by joint instability. This might be because the former 3 disorders are associated with inflammation while the latter are degenerative conditions, and both mPGES-1 and PGE_2 play important roles in inflammatory reactions. In fact, not only CIA and LPS-induced bone loss but also fracture healing are known to be initiated in response to regulatory factors associated with inflammation and the innate immune response (34).

Alternatively, the discrepancy in the effects of mPGES-1 deficiency might be attributable to differing compensatory mechanisms in response to the deficiency, similar to the observations in COX-2$^{-/-}$ mice indicating that primary hyperparathyroidism could develop (35,36). Since CIA, LPS-induced bone loss, and fracture healing progress more rapidly than ovariectomy- or unloading-induced bone loss and stress-induced OA, it is likely that any mechanism of compensation would not be adequate for the former disorders but would be sufficient to countervail the latter.

Following bone fracture, a sequence of events regulated by various molecules is induced to bring about endochondral and intramembranous bone formation (34). In fact, by creating the same model of bone fracture in knockout mice as used in the present study, we previously found that insulin receptor substrate 1, carminerin, and matrix metalloproteinase 13 had great effect on the stages of chondrocyte proliferation, calcification, and cartilage resorption, respectively, during endochondral bone formation (30,32,37). Although, in the present study, mPGES-1 was shown to be expressed during both endochondral and intramembranous bone formation (Figure 3B), the most prominent abnormality of the callus of mPGES-1$^{-/-}$ mice was the reduced quantity of cartilaginous tissue (Figure 5A).

In addition, further in vivo and ex vivo analyses showed that proliferation of mPGES-1$^{-/-}$ chondrocytes was suppressed; however, interestingly, the suppression was more conspicuous in vivo than ex vivo (Figures 5A and B). This might be due to differences in the nutritional environment, i.e., the in vivo chondrocytes were surrounded by avascular cartilage matrix, whereas cultured chondrocytes were in a nutritious medium that contained compensatory factors in response to the proliferation. The increase in mPGES-1 expression was associated with an increase in PGE_2 production in the fracture callus (Figures 3C and D), as we have also reported previously in conditions of LPS stimulation and arthritis induction (6), and PGE_2 is known to stimulate the proliferation of chondrocytes via the EP1 receptor (38).

Similar to our present findings in mPGES-1$^{-/-}$ mice, COX-2$^{-/-}$ mice are reported to exhibit impaired fracture healing (19,20). However, the mechanism underlying the impaired fracture healing in COX-2$^{-/-}$ mice is an unresolved issue, and may be different from that in mPGES-1$^{-/-}$ mice. It has been proposed that the mechanism of impairment is a suppression of terminal differentiation of chondrocytes during endochondral bone formation (20), whereas others have reported that the mechanism might be a reduction in osteoblastic differentiation from immature mesenchymal cells during both endochondral and intramembranous bone formation, induced via decreases in 2 essential genes, Runx2 and osterix (19). The present culture experiments revealed that differentiation of chondrocytes was not affected by the deficiency of mPGES-1 (Figure 5C). Moreover, in our preliminary culture experiment using mPGES-1$^{-/-}$ bone marrow stromal cells, we found that there were no abnormalities in osteoblastogenesis or in the expression of Runx2 and osterix (results not shown). Therefore, the critical cells or differentiation stages related to the contributions of COX-2 and mPGES-1 could be different, and would thus explain the differences in the way in which PGE_2 regulates bone formation (1).

In addition, the transcriptional mechanisms of induction of COX-2 and mPGES-1 are not identical. COX-2 is known to be induced by the transcription factors NF-κB, NF-IL6, activator protein 1, CCAAT/enhancer binding protein α (C/EBPα), C/EBPβ, cAMP response element, and Runx2 (39), while mPGES-1 is mainly transactivated by Egr-1 via MAPK pathways such as ERK-1/2 and p38 (40). Thus, even though COX-2 and mPGES-1 are stimulus-inducible and function sequentially in the same PGE_2-biosynthetic pathway, they appear to have less in common in their upstream and downstream signaling pathways.

Nonsteroidal antiinflammatory drugs (NSAIDs) and selective COX-2 inhibitors have recently been shown to inhibit bone repair in animal models and

clinical studies, although these findings have been obtained only retrospectively (41,42). More importantly, specific COX-2 inhibitors have been reported to increase the risk of cardiovascular events in patients in clinical trials, although whether this is a common risk factor of COX-2–selective agents or could be attributed to NSAIDs more generally is still under debate (43). The increase in cardiovascular events may be due to inhibition of PGI_2, which results in vasodilatory and platelet-inhibitory effects and can lead to detrimental effects on coagulation control (43).

Unlike NSAIDs and COX-2 inhibitors, which suppress not only PGE_2 but also other PGs that play essential roles in physiologic functions, specific mPGES-1 inhibitors are expected to function as highly selective agents in the management of several disorders. In fact, it has been observed that mPGES-$1^{-/-}$ mice exhibit no alterations in thrombogenesis or blood pressure, whereas selective COX-2 inhibitors have been associated with these effects (44). Furthermore, mPGES-$1^{-/-}$ mice lack the renal dysfunction and failure of the female reproductive system that has been seen in COX-$2^{-/-}$ mice (45).

These findings suggest that the mPGES-1 enzyme may represent a treatment target that could be manipulated without affecting important physiologic systems in which other PGs are involved. However, implementation of this treatment strategy will still require caution, because, in addition to its detrimental functions, PGE_2 also exerts homeostatic and defensive effects in several organs, such as the gastrointestinal tract, lung, and kidney, as well as in bone repair, as shown herein. Although selective mPGES-1 inhibitors have recently been developed (46) as a replacement for NSAIDs and COX-2 inhibitors, deliberate randomized and controlled clinical trials will be essential to determine the effectiveness of this new treatment approach.

AUTHOR CONTRIBUTIONS

Dr. Kawaguchi had full access to all of the data in the study and takes responsibility for the integrity of the data and the accuracy of the data analysis.

Study design. Yamakawa, Kudo, Akira, Nakamura, Kawaguchi.

Acquisition of data. Yamakawa, Kamekura, Kamei, Murakami, Uematsu.

Analysis and interpretation of data. Yamakawa, Saegusa, Chung, Kawaguchi.

Manuscript preparation. Yamakawa, Kawamura, Kawaguchi.

Statistical analysis. Yamakawa, Kamekura.

REFERENCES

1. Kawaguchi H, Pilbeam CC, Harrison JR, Raisz LG. The role of prostaglandins in the regulation of bone metabolism. Clin Orthop Relat Res 1995;313:36–46.
2. Kobayashi T, Narumiya S. Function of prostanoid receptors: studies on knockout mice. Prostaglandins Other Lipid Mediat 2002;68-69:557–73.
3. Murakami M, Kudo I. Recent advances in molecular biology and physiology of the prostaglandin E_2-biosynthetic pathway. Prog Lipid Res 2004;43:3–35.
4. Murakami M, Naraba H, Tanioka T, Semmyo N, Nakatani Y, Kojima F, et al. Regulation of prostaglandin E_2 biosynthesis by inducible membrane-associated prostaglandin E_2 synthase that acts in concert with cyclooxygenase-2. J Biol Chem 2000;275: 32783–92.
5. Jakobsson PJ, Thoren S, Morgenstern R, Samuelsson B. Identification of human prostaglandin E synthase: a microsomal, glutathione-dependent, inducible enzyme, constituting a potential novel drug target. Proc Natl Acad Sci U S A 1999;96:7220–5.
6. Kamei D, Murakami M, Nakatani Y, Ishikawa Y, Ishii T, Kudo I. Potential role of microsomal prostaglandin E synthase-1 in tumorigenesis. J Biol Chem 2003;278:19396–405.
7. Naraba H, Yokoyama C, Tago N, Murakami M, Kudo I, Fueki M, et al. Transcriptional regulation of the membrane-associated prostaglandin E2 synthase gene: essential role of the transcription factor Egr-1. J Biol Chem 2002;277:28601–8.
8. Tanikawa N, Ohmiya Y, Ohkubo H, Hashimoto K, Kanagawa K, Kojima M, et al. Identification and characterization of a novel type of membrane-associated prostaglandin E synthase. Biochem Biophys Res Commun 2002;291:884–9.
9. Murakami M, Nakashima K, Kamei D, Masuda S, Ishikawa Y, Ishii T, et al. Cellular prostaglandin E_2 production by membrane-bound prostaglandin E synthase-2 via both cyclooxygenases-1 and -2. J Biol Chem 2003;278:37937–47.
10. Saegusa M, Murakami M, Nakatani Y, Yamakawa K, Katagiri M, Matsuda K, et al. Contribution of membrane-associated prostaglandin E_2 synthase to bone resorption. J Cell Physiol 2003;197: 348–56.
11. Tanioka T, Nakatani Y, Semmyo N, Murakami M, Kudo I. Molecular identification of cytosolic prostaglandin E_2 synthase that is functionally coupled with cyclooxygenase-1 in immediate prostaglandin E_2 biosynthesis. J Biol Chem 2000;275:32775–82.
12. Tanioka T, Nakatani Y, Kobayashi T, Tsujimoto M, Oh-ishi S, Murakami M, et al. Regulation of cytosolic prostaglandin E_2 synthase by 90-kDa heat shock protein. Biochem Biophys Res Commun 2003;303:1018–23.
13. Uematsu S, Matsumoto M, Takeda K, Akira S. Lipopolysaccharide-dependent prostaglandin E_2 production is regulated by the glutathione-dependent prostaglandin E_2 synthase gene induced by the Toll-like receptor 4/MyD88/NF-IL6 pathway. J Immunol 2002; 168:5811–6.
14. Trebino CE, Stock JL, Gibbons CP, Naiman BM, Wachtmann TS, Umland JP, et al. Impaired inflammatory and pain responses in mice lacking an inducible prostaglandin E synthase. Proc Natl Acad Sci U S A 2003;100:9044–9.
15. Kamei D, Yamakawa K, Takegoshi Y, Mikami-Nakanishi M, Nakatani Y, Oh-ishi S, et al. Reduced pain hypersensitivity and inflammation in mice lacking microsomal prostaglandin E synthase-1. J Biol Chem 2004;279:33684–95.
16. Okada Y, Lorenzo JA, Freeman AM, Tomita M, Morham SG, Raisz LG, et al. Prostaglandin G/H synthase-2 is required for maximal formation of osteoclast-like cells in culture. J Clin Invest 2000;105:823–32.
17. Inada M, Matsumoto C, Uematsu S, Akira S, Miyaura C. Membrane-bound prostaglandin E synthase-1-mediated prostaglandin E_2 production by osteoblast plays a critical role in lipopolysaccharide-induced bone loss associated with inflammation. J Immunol 2006;177:1879–85.
18. Paralkar VM, Borovecki F, Ke HZ, Cameron KO, Lefker B, Grasser WA, et al. An E_2 receptor-selective prostaglandin E_2

agonist induces bone healing. Proc Natl Acad Sci U S A 2003;100: 6736–40.
19. Zhang X, Schwarz EM, Young DA, Puzas JE, Rosier RN, O'Keefe RJ. Cyclooxygenase-2 regulates mesenchymal cell differentiation into the osteoblast lineage and is critically involved in bone repair [published erratum appears in J Clin Invest 2002;110:1211]. J Clin Invest 2002;109:1405–15.
20. Simon AM, Manigrasso MB, O'Connor JP. Cyclo-oxygenase 2 function is essential for bone fracture healing. J Bone Miner Res 2002;17:963–76.
21. Goldring MB, Berenbaum F. The regulation of chondrocyte function by proinflammatory mediators: prostaglandins and nitric oxide. Clin Orthop Relat Res 2004:S37–46.
22. Laufer S. Role of eicosanoids in structural degradation in osteoarthritis. Curr Opin Rheumatol 2003;15:623–7.
23. Hardy MM, Seibert K, Manning PT, Currie MG, Woerner BM, Edwards D, et al. Cyclooxygenase 2–dependent prostaglandin E_2 modulates cartilage proteoglycan degradation in human osteoarthritis explants. Arthritis Rheum 2002;46:1789–803.
24. Miwa M, Saura R, Hirata S, Hayashi Y, Mizuno K, Itoh H. Induction of apoptosis in bovine articular chondrocyte by prostaglandin E_2 through cAMP-dependent pathway. Osteoarthritis Cartilage 2000;8:17–24.
25. McCoy JM, Wicks JR, Audoly LP. The role of prostaglandin E_2 receptors in the pathogenesis of rheumatoid arthritis. J Clin Invest 2002;110:651–8.
26. Jacques C, Sautet A, Moldovan M, Thomas B, Humbert L, Berenbaum F. Cyclooxygenase activity in chondrocytes from osteoarthritic and healthy cartilage. Rev Rhum Engl Ed 1999;66: 701–4.
27. Kojima F, Naraba H, Miyamoto S, Beppu M, Aoki H, Kawai S. Membrane-associated prostaglandin E synthase-1 is upregulated by proinflammatory cytokines in chondrocytes from patients with osteoarthritis. Arthritis Res Ther 2004;6:R355–65.
28. Akune T, Ohba S, Kamekura S, Yamaguchi M, Chung UI, Kubota N, et al. PPARγ insufficiency enhances osteogenesis through osteoblast formation from bone marrow progenitors. J Clin Invest 2004;113:846–55.
29. Kamekura S, Hoshi K, Shimoaka T, Chung U, Chikuda H, Yamada T, et al. Osteoarthritis development in novel experimental mouse models induced by knee joint instability. Osteoarthritis Cartilage 2005;13:632–41.
30. Yamada T, Kawano H, Koshizuka Y, Fukuda T, Yoshimura K, Kamekura S, et al. Carminerin contributes to chondrocyte calcification during endochondral ossification. Nat Med 2006;12:665–70.
31. Kamekura S, Kawasaki Y, Hoshi K, Shimoaka T, Chikuda H, Maruyama Z, et al. Contribution of runt-related transcription factor 2 to the pathogenesis of osteoarthritis in mice after induction of knee joint instability. Arthritis Rheum 2006;54:2462–70.
32. Shimoaka T, Kamekura S, Chikuda H, Hoshi K, Chung UI, Akune T, et al. Impairment of bone healing by insulin receptor substrate-1 deficiency. J Biol Chem 2004;279:15314–22.
33. Van Griensven M, Lobenhoffer P, Barke A, Tschernig T, Lindenmaier W, Krettek C, et al. Adenoviral gene transfer in a rat fracture model. Lab Anim 2002;36:455–61.
34. Barnes GL, Kostenuik PJ, Gerstenfeld LC, Einhorn TA. Growth factor regulation of fracture repair. J Bone Miner Res 1999;14: 1805–15.
35. Xu M, Choudhary S, Goltzman D, Ledgard F, Adams D, Gronowicz G, et al. Do cyclooxygenase-2 knockout mice have primary hyperparathyroidism? Endocrinology 2005;146:1843–53.
36. Myers LK, Bhattacharya SD, Herring PA, Xing Z, Goorha S, Smith RA, et al. The isozyme-specific effects of cyclooxygenase-deficiency on bone in mice. Bone 2006;39:1048–52.
37. Kosaki N, Takaishi H, Kamekura S, Kimura T, Okada Y, Minqi L, et al. Impaired bone fracture healing in matrix metalloproteinase-13 deficient mice. Biochem Biophys Res Commun 2007;354: 846–51.
38. Brochhausen C, Neuland P, Kirkpatrick CJ, Nusing RM, Klaus G. Cyclooxygenases and prostaglandin E_2 receptors in growth plate chondrocytes in vitro and in situ: prostaglandin E2 dependent proliferation of growth plate chondrocytes. Arthritis Res Ther 2006;8:R78.
39. Chikazu D, Li X, Kawaguchi H, Sakuma Y, Voznesensky OS, Adams DJ, et al. Bone morphogenetic protein 2 induces cyclooxygenase 2 in osteoblasts via a Cbfal binding site: role in effects of bone morphogenetic protein 2 in vitro and in vivo. J Bone Miner Res 2002;17:1430–40.
40. Masuko-Hongo K, Berenbaum F, Humbert L, Salvat C, Goldring MB, Thirion S. Up-regulation of microsomal prostaglandin E synthase 1 in osteoarthritic human cartilage: critical roles of the ERK-1/2 and p38 signaling pathways. Arthritis Rheum 2004;50: 2829–38.
41. Giannoudis PV, MacDonald DA, Matthews SJ, Smith RM, Furlong AJ, De Boer P. Nonunion of the femoral diaphysis: the influence of reaming and non-steroidal anti-inflammatory drugs. J Bone Joint Surg Br 2000;82:655–8.
42. Gerstenfeld LC, Al-Ghawas M, Alkhiary YM, Cullinane DM, Krall EA, Fitch JL, et al. Selective and nonselective cyclooxygenase-2 inhibitors and experimental fracture-healing: reversibility of effects after short-term treatment. J Bone Joint Surg Am 2007;89: 114–25.
43. Dieppe PA, Ebrahim S, Martin RM, Juni P. Lessons from the withdrawal of rofecoxib. BMJ 2004;329:867–8.
44. Cheng Y, Wang M, Yu Y, Lawson J, Funk CD, Fitzgerald GA. Cyclooxygenases, microsomal prostaglandin E synthase-1, and cardiovascular function. J Clin Invest 2006;116:1391–9.
45. Langenbach R, Loftin C, Lee C, Tiano H. Cyclooxygenase knockout mice: models for elucidating isoform-specific functions. Biochem Pharmacol 1999;58:1237–46.
46. Riendeau D, Aspiotis R, Ethier D, Gareau Y, Grimm EL, Guay J, et al. Inhibitors of the inducible microsomal prostaglandin E_2 synthase (mPGES-1) derived from MK-886. Bioorg Med Chem Lett 2005;15:3352–5.

Osteoporos Int (2008) 19:21–28
DOI 10.1007/s00198-007-0474-1

ORIGINAL ARTICLE

Association between height loss and bone loss, cumulative incidence of vertebral fractures and future quality of life: the Miyama study

N. Yoshimura · H. Kinoshita · T. Takijiri · H. Oka · S. Muraki · A. Mabuchi · H. Kawaguchi · K. Nakamura · T. Nakamura

Received: 23 January 2007 / Accepted: 22 May 2007 / Published online: 26 October 2007

Abstract
Introduction The study aimed to clarify associations between height loss, bone loss and the quality of life (QOL) score among general inhabitants of Miyama, a rural Japanese community. This population-based epidemiological study was conducted in Miyama, a village located in a mountain area in Wakayama Prefecture, Japan.

Methods A list of all inhabitants comprising 1,543 inhabitants (716 men, 827 women) born in this village between 1910–1949 was compiled. From the above whole cohort, a subcohort to measure bone mineral density (BMD) was recruited, consisting of 400 participants, divided into four groups of 50 men and 50 women each, and stratified into age decades by decade of birth-year (1910–1919, 1920–1929, 1930–1939 or 1940–1949). BMD measurement, physical measurements of height (cm) and body weight (kg) were taken, and body mass index (BMI; kg/m^2) were calculated. BMD and anthropometric measurements were repeated on the same participants at 3, 7 and 10 years after baseline measurement (1993, 1997 and 2000).
Results and discussion Among 299 of 400 participants, changes in height over 10 years for men in their 40s, 50s, 60s and 70s were −0.7 cm, −0.5 cm, −1.2 cm and −1.5 cm, respectively, compared with −0.7 cm, −1.4 cm, −2.1 cm and −3.7 cm in women, respectively. No significant relationships between change in height and rate of change in BMD at the lumbar spine and femoral neck after adjustment for age in men (lumbar spine, β=0.058, standard error of the mean (SE)=0.031, P=0.501, R^2= 0.038; femoral neck, β=0.100, SE=0.038, P=0.228, R^2= 0.121) were identified. By contrast, among women, a significant positive association was identified between height change and change rate of BMD at the lumbar spine after adjusting for age (β=0.221, SE=0.039, P=0.012, R^2= 0.069), while no significant relationship was found between height change and change rate at the femoral neck (β=0.107, SE=0.039, P=0.229, R^2=0.048). No significant relationship was noted between vertebral fractures (VFx) and height at baseline in men and women (men: odds ratio (OR) 0.93, 95% confidence interval (CI) 0.81–1.05, P=0.24; women: OR 0.97, 95% CI 0.87–1.08, P=0.58) or between VFx and height loss

N. Yoshimura (✉) · H. Oka
Department of Joint Disease Research,
22nd Century Medical and Research Center,
Graduate School of Medicine, University of Tokyo,
7-3-1 Hongo, Bunkyo-ku,
Tokyo 113-8655, Japan
e-mail: yoshimuran-ort@h.u-tokyo.ac.jp

H. Kinoshita
Department of Orthopaedic Surgery, Wakayama Medical University Kihoku Hospital,
Wakayama, Japan

T. Takijiri
Public Health Center, Hidakagawa Town Council,
Wakayama, Japan

S. Muraki · A. Mabuchi
Department of Clinical Motor System Medicine,
22nd Century Medical and Research Center,
Graduate School of Medicine, University of Tokyo,
Tokyo, Japan

H. Kawaguchi · K. Nakamura
Department of Orthopaedic Surgery, Faculty of Medicine,
University of Tokyo,
Tokyo, Japan

T. Nakamura
Department of Orthopedic Surgery,
University of Occupational and Environmental Health,
Fukuoka, Japan

(men: OR 1.31, 95% CI 1.00–1.71, P=0.051; women: OR 1.20, 95% CI 0.94–1.53, P=0.14). In both men and women, no significant relationship was identified between utility of the EuroQol EQ5D questionnaire and height at baseline (men: β=−0.148, SE=0.003, P=0.202, R^2=0.076; women: β=0.127, SE=0.004, P=0.235, R^2=0.048), and height change (men: β=−0.078, SE=0.008, P=0.452, R^2=0.065; women: β=0.053, SE=0.010, P=0.608, R^2=0.038).

Keywords Bone mineral density · Cohort study · Height loss · Osteoporosis · Quality of life · Vertebral fractures

Introduction

Osteoporotic fracture is one of the leading reasons for the elderly becoming bedridden in Japan [1, 2]. Among fractures associated with osteoporosis, hip fracture results in confinement to bed and markedly impaired quality of life (QOL) in aged individuals. The number of patients with femoral neck fracture has almost doubled over the past 15 years from 1987 to 2002 [3, 4]. Prevention of osteoporosis and osteoporotic fracture is, therefore, an urgent issue for maintaining QOL in the elderly and containing the medical costs of their care.

For the prevention of osteoporosis, the importance of risk assessment must be emphasized. As a risk factor of osteoporosis and osteoporotic fractures, anthropometric measurements no doubt have an important role to play. Particularly among anthropometric measures, light weight [5–8], weight loss [9, 10], and low body mass index (BMI) [11–13] suggest a risk of osteoporosis and osteoporotic fractures. However, data are scarcer on relationships between height loss and subsequent rate of changes in bone mineral density (BMD) or osteoporotic fractures. In addition, few reports have assessed relationships between height loss and subsequent loss of QOL.

To clarify associations between height or height loss and bone loss, osteoporotic fractures focused on vertebral fractures and QOL scores among general inhabitants, the present study was performed as a postal survey on the cohort established in Miyama, a rural Japanese community.

Methods

Establishment of baseline cohort

This population-based epidemiological study was initiated in 1990 in Miyama, a mountain village in Wakayama Prefecture, Japan. As the Miyama cohort has been profiled in detail elsewhere [14, 15], subject characteristics are summarized here briefly. A list of all inhabitants born in this village between 1910–1949, and therefore aged 40 to 79 years, was compiled from the register of residents as of the end of 1989. A cohort of 1,543 inhabitants (716 men, 827 women) was identified, all of whom completed a self-administered questionnaire covering daily activities, such as dietary habits, smoking habits, alcohol consumption and physical exercise (125 items) (the whole cohort).

From the above whole cohort, a BMD cohort was recruited, consisting of 400 participants, divided into four groups of 50 men and 50 women each, and stratified into age decades by decade of birth-year (1910–1919, 1920–1929, 1930–1939, 1940–1949). An interviewer administered a second questionnaire to these 400 participants, covering items of past medical history, family history, calcium intake, dietary habits, physical exercise, occupational activities and sun exposure, in addition to reproductive variables for women.

BMD and anthropometric measurements

The baseline measurement of BMD was made in 1990. Dual energy X-ray absorptiometry (DXA:Lunar DPX, Madison, WI, USA) was used for the measurement of BMD, providing antero-posterior images at lumbar vertebrae L2–4 and the proximal femur (femoral neck, Ward's triangle, trochanter, and total hip). In addition to BMD, physical measurements of height and body weight were taken, and BMI (kg/m^2) was calculated. Height and weight at each visit were all measured by the same well-trained public health nurse (TT).

BMD measurements were repeated on the same participants at 3, 7 and 10 years after baseline measurement (1993, 1997 and 2000). Rates of change in BMD and height change were calculated over the 10-year period, classified by sex and age stratum. BMD measurements at all visits were performed by the same well-trained medical doctor (NY).

To control for precision of DXA, the equipment was checked every examination in 1990, 1993, 1997 and 2000 using the same phantom, and BMD of the phantom was regulated to 1.270 ±0.025 g/cm^2 (2%) during examinations. In addition, to control for observer variability, all participants were examined by the same medical doctor. Intra-observer variability of DXA (Lunar DPX) in vitro and in vivo had been measured for a prior study [16], using the same doctor, and CV% for L2–4 in vitro was determined as 0.35%, while CV% for L2–4, proximal femur, Ward's triangle and trochanter, examined in vivo in five male volunteers, were 0.61–0.90%, 1.02–2.57%, 1.97–5.45% and 1.77–4.17%, respectively.

Radiography

Radiographic examination of the spine was performed on all participants in 1990. Anteroposterior and lateral images

of thoracolumbar vertebrae Th5-L5 were used for diagnosis (Initial X-ray survey). Radiographic examination was again performed on subjects who provided consent after 10 years. Lateral images of thoracolumbar vertebrae Th5-L5 were again used for diagnosis (2nd X-ray survey). Lateral spinal radiographs were examined for the presence of one or more vertebral fractures (VFx) between Th5–L5, using the criteria determined by the Japan Bone and Mineral Society (Fig. 1) [17]. According to these criteria, measurement of anterior, middle and posterior heights on lateral radiography of the thoracic and lumbar spine is required, to determine ratios defining the anterior wedge, biconcave and compound dimensions of the vertebral bodies. Diagnosis of VFx on all radiographs was performed by the same experienced orthopedic doctor (HK). In the present study, cumulative incidence over 10 years was detected by dividing the number of incident cases by the number of participants in the follow-up study, and cases with previous VFx were excluded from both numerators and denominators. In this analysis, cumulative incidence of cases with first VFx was detected.

QOL postal survey

The QOL questionnaire postal survey was performed in 2002. To select QOL items, the Euro Qol EQ5D questionnaire [18] translated into Japanese was used, comprising the following two parts: a 5-dimensional health state classification; and a visual analogue scale (VAS) called the "thermometer" [19]. The 5-dimensional healthcare classification included questions on the status of morbidity, self-care, usual activities, pain/discomfort and anxiety/depression. Participants were asked to indicate current health status by ticking the most appropriate of three statements about each of five QOL dimensions. Each statement represents an increasing degree of severity. These results were coded and converted to a score of utility using the tables of values. The VAS "thermometer" represents a self-rated scale of current health-related QOL. The endpoint of 100 at the top indicates the best imaginable health state, and 0 at the bottom indicates the worst imaginable health state at that time.

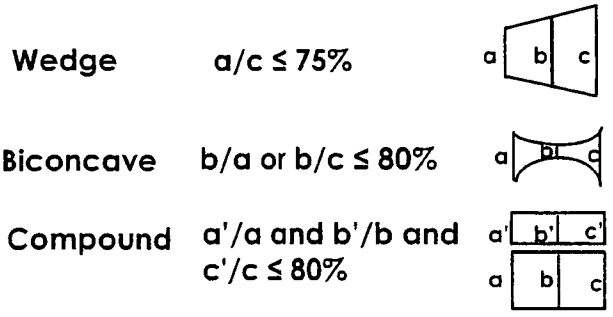

Fig. 1 Diagnostic criteria of vertebral fractures

Statistical analysis

Statistical analyses were performed using SPSS statistical software (SPSS, USA) and STATA software (STATA, USA). Differences were tested for significance using ANOVA for comparison among multiple groups and Scheffe's LSD test for pairs of groups. Significant items were selected, and multiple regression analysis was performed with adjustment of suitable variables.

Results

Eligible participants

From the whole cohort of 1,543 inhabitants (716 men, 827 women), 50 men and 50 women in each decade age group between 40–79 years (a total of 400 participants) were recruited for baseline bone densitometry in 1990 (baseline BMD cohort).

To evaluate the representativeness of subjects in the baseline BMD cohort compared to the whole cohort, the prevalence of 125 items of the self-administered questionnaire, results of physical measurements and blood examination were compared between members of the BMD and whole cohorts [14]. As a result, prevalence of lifestyle factors such as smoking and drinking were identical among BMD and whole cohorts. In addition, no significant differences existed in frequency distribution of the following items favorable to the maintenance of good health among BMD and whole cohorts: sleeping 7–8 h/day; exercise and sports >1 h/day; walking >30 min/day; eating regularly; reduction of salt intake compared with age 30; less stress; less anger. Regarding medical examinations, no significant differences in blood pressure classified by age and sex were seen between cohorts. Moreover, no abnormal values in serum calcium or phosphorus were observed. In view of these findings, subjects in the BMD study were considered to have been selected adequately from the whole cohort.

A total of 299 of 400 participants (137 men, 162 women; 74.8%) completed the follow-up survey after 10 years. Loss of 101 participants was due to following: death, n=55 (37 men, 18 women); moved away from Miyama, n=16 (8 men, 8 women); illness, n=13 (4 men, 9 women); busy, n=8 (8 men); refused to participate further, n=5 (5 men); and away from the area at the time of follow-up, n=4 (1 man, 3 women). Analysis was performed on the 299 subjects who had participated in all surveys performed in 1990, 1993, 1997 and 2000.

A comparison of physical characteristics between completers and non-completers has been described elsewhere [20], and is briefly summarized here. Height, weight and